THE GEOLOGICAL SOCIETY OF AMERICA®

Progressive northward growth of the northern Qilian Shan–Hexi Corridor (northeastern Tibet) during the Cenozoic

Dewen Zheng[1], Weitao Wang[1,*], Jinglin Wan[1], Daoyang Yuan[2], Chunru Liu[1], Wenjun Zheng[1,3], Huiping Zhang[1], Jianzhang Pang[1], and Peizhen Zhang[1,3]

[1]STATE KEY LABORATORY OF EARTHQUAKE DYNAMICS, INSTITUTE OF GEOLOGY, CHINA EARTHQUAKE ADMINISTRATION, YARD NO. 1, HUA YAN LI, CHAOYANG DISTRICT, BEIJING, CHINA
[2]INSTITUTE OF LANZHOU SEISMOLOGY, CHINA EARTHQUAKE ADMINISTRATION, LANZHOU 730000, CHINA
[3]SCHOOL OF EARTH SCIENCE AND GEOLOGICAL ENGINEERING, SUN YAN-SEN UNIVERSITY, GUANGZHOU, 510275, CHINA

ABSTRACT

The uplift processes of the Qilian Shan (northern Tibetan Plateau) play a central role in our understanding of the dynamics of outward and upward growth of Tibet due to sustained convergence of the Indian and Asian plates. We employ apatite fission track chronology and geological mapping to reveal the time and pattern of the deformation along the Qilian Shan. Our results indicate that the emergence of the Tuolai Shan in the central Qilian Shan occurred at 17–14 Ma, that northern Qilian Shan thrusting began at 10–8 Ma, and that the Laojunmiao anticline formed ca. 3.6 Ma. Together with previous results that show that uplift of the southern Qilian Shan began in the Oligocene, we suggest that the Qilian Shan has undergone progressively northward expansion in the Cenozoic due to significant crustal shortening driven by Qilian Shan thrust fault systems.

LITHOSPHERE; v. 9; no. 3; p. 408–416 | Published online 20 March 2017 doi:10.1130/L587.1

INTRODUCTION

The most impressive consequence of the collision between the Indian and Asian continents is the formation of the Tibetan Plateau, which resulted from large-scale crustal thickening and lateral expansion of high terrain. Although the plateau has been studied for decades, the mechanism of upward and outward growth of the Tibetan Plateau and the environmental feedback resulting from the appearance of the high plateau are debated (An et al., 2001; Clark, 2012; Hough et al., 2011; Molnar et al., 1993, 2010; Royden et al., 1997, 2008; Tapponnier et al., 2001). Revealing when and how the Tibetan Plateau reached its present elevation and lateral extension can provide significant constraints on the mechanism of Tibetan Plateau growth (Clark, 2012; Clark et al., 2010; Wang et al., 2013, 2016b; Zheng et al., 2006).

The Qilian Shan is the largest mountain belt in the northern Tibet Plateau (length >1000 km, width ~270 km, mean elevation ~4000 m, highest peak ~5500 m) and marks the geomorphic north of the Tibetan Plateau (Fig. 1). The Qilian Shan is the latest region involved in Tibetan Plateau growth (Tapponnier et al., 2001) and underwent distributed shortening deformation (Hetzel et al., 2004; Zhang et al., 2004). The total shortening rate across the Qilian Shan is ~5–7 mm/yr, and is distributed across five parallel active faults (Champagnac et al., 2010; Hetzel et al., 2004; Palumbo et al., 2009; Yuan et al., 2004; Zhang et al., 2004). Thrusting in the Qilian Shan has been linked to crustal thickening and topographic growth due to the accommodation of left-lateral displacement along the Altyn Tagh fault (Burchfiel et al., 1989; Métivier et al., 1998; Meyer et al., 1998; Wang et al., 2016a; Yue et al., 2001, 2004). Therefore, temporal and spatial deformational patterns of the Qilian Shan play a central role in exploring the mechanism of Tibetan Plateau growth. Despite progress, the deformational history of the Qilian Shan is debated, and initial growth of the Qilian Shan ranges from early Eocene to Pliocene (Dupont-Nivet et al., 2004; Fang et al., 2005, 2007; George et al., 2001; Horton et al., 2004; Jolivet et al., 2001; Métivier et al., 1998; Wang et al., 2016a, 2016b, 2016c; Yin et al., 2008, 2002; Zheng et al., 2010). For example, Cenozoic tectonic evolution of the Qaidam Basin in the south flank of the Qilian Shan requires Eocene uplift of the range to provide the clasts for the basin (Yin et al., 2008). However, recognition of an unconformity within the Hexi Corridor basin dated by paleomagnetic correlation suggests that thrusting in the Qilian Shan has occurred since the late Miocene (ca. 8 Ma), but the most intensive deformation probably occurred at 4–3 Ma, because the thick conglomerates were deposited along the region during this time interval (Fang et al., 2005). Instead of uplift driving deposition of the thick conglomerates, it was suggested (Zhang et al., 2001) that the conglomerates deposited 4–2 Ma in the north margin of the Qilian Shan may result from a period of frequently changing climate. Apatite helium data collected along vertical section indicate that the northern Qilian Shan thrusting began ca. 9.5 Ma (Zheng et al., 2010), Laji Shan thrusting began ca. 22 Ma, and Jishi Shan thrusting began ca. 13 Ma (Lease et al., 2012). Moreover, Palumbo et al. (2010) suggested that initial growth of the Yumu Shan (the most frontal branch of the Qilian Shan) took place ca. 4–3 Ma based on the wind gap migration and cosmogenic nuclide ^{10}Be dating.

Regionally, more complex deformation and sparse studies may be the reasons why the deformation time and style of the Qilian Shan have been

Weitao Wang http://orcid.org/0000-0002-4849-8325
*Corresponding author

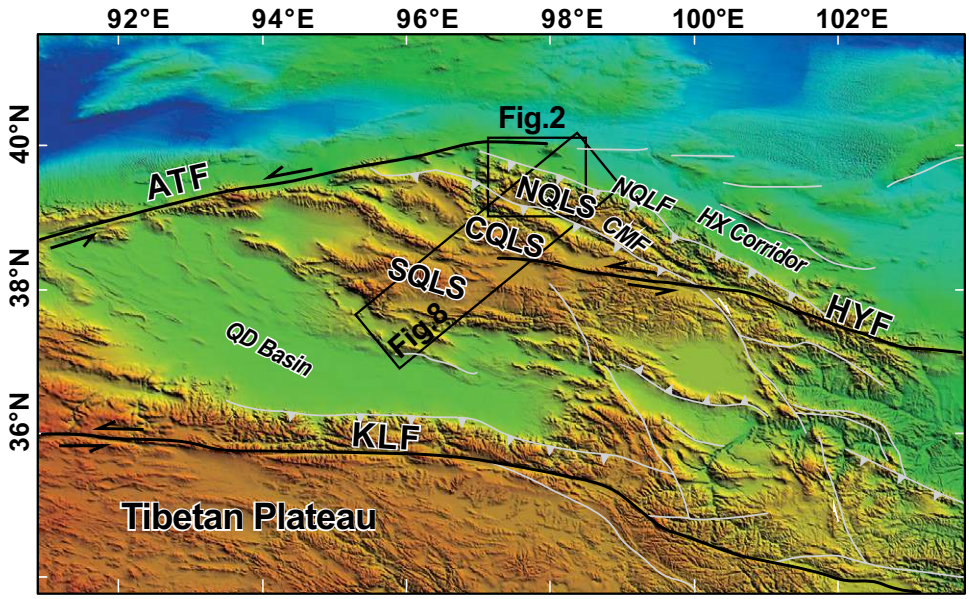

Figure 1. A digital elevation map of the northeast Tibetan Plateau showing the topographic features of the Qilian Shan and location of the Qaidam Basin and Hexi Corridor basin in the south and north flanks of the Qilian Shan, respectively. SQLS—southern Qilian Shan, CQLS—central Qilian Shan, NQLS—northern Qilian Shan, ATF—Altyn Tagh fault, KLF—Kunlun fault, HYF—Haiyuan fault, CMF—Changma fault, NQLF—northern Qilian fault, HX—Hexi, QD—Qaidam.

debated, and highlight the need for further studies in order to determine the deformation pattern in detail. Our apatite fission track (AFT) data and mapping of the deformed strata related to the northern Qilian Shan thrust fault system indicate that deformation along the northern Qilian Shan has propagated progressively to the north from the middle to late Miocene.

GEOLOGICAL SETTING

The Qilian Shan is a Caledonian orogenic belt and has been divided into three structural units: the northern, central, and southern Qilian Shan (Xiao et al., 2009; Yin and Harrison, 2000). The northern and central Qilian Shan are complex Paleozoic arc systems that are separated by a high-pressure metamorphic belt containing blueschist and ophiolite. The southern Qilian Shan consists of Ordovician to Silurian sedimentary rocks and probable early Paleozoic basement (Gansu Bureau of Geology and Mineral Resources, 1989). During the Mesozoic, the Qilian Shan region underwent large-scale extension and developed thick Jurassic–Cretaceous continental strata. After a phase of relative quiescence, the faults across the Qilian Shan were reactivated and thrusted both sides to the Qaidam Basin in the south and to the Hexi Corridor basin in the north during the Cenozoic (Fig. 1).

The Qilian Shan defines the modern northeastern boundary of the Tibetan Plateau, which contains peak elevations to ~5500 m and surface elevations of ~4000 m (Fig. 1). To the south, the Qaidam Basin is a relatively low relief surface of ~2800 m elevation with >10-km-thick Cenozoic terrigenous sediments. To the north, the Hexi Corridor basin overlies the stable Alax block with a much lower surface (1500–2000 m in elevation) and >2-km-thick Cenozoic terrigenous sediments (Fig. 2).

The Cenozoic tectonics of the Qilian Shan and its adjacent regions are characterized by folds, thrust faults, and strike-slip faults that partially accommodate India-Eurasia plate convergence (Molnar and Tapponnier, 1975; Tapponnier et al., 2001; Zheng et al., 2013a). The geodetic shortening rate is 5–7 mm/yr (Zhang et al., 2004) between the Qaidam and the Alax block and there are active thrust faults throughout the region (Hetzel et al., 2004; Métivier et al., 1998; Yuan et al., 2013; Zheng et al., 2013b). The northern Qilian Shan thrust juxtaposes low-grade metamorphic early Paleozoic rocks (slates, phyllites, limestones, and volcanic and granitic rocks) over Cenozoic sediments within the Hexi Corridor basin (Fig. 2).

Cenozoic strata in the Hexi corridor are 2000–3000 m thick and are divided into five primary stratigraphic units, from bottom to top, the Huoshaogou, Baiyanghe, and Shulehe Formations and the Yumen and Jiuquan conglomerates (Gansu Bureau of Geology and Mineral Resources, 1989; Fang et al., 2005; Wang et al., 2016a).The Huoshaogou Formation represents the oldest deposits in the Hexi Corridor basin, which is characterized by alluvial conglomerate and braided fluvial purple-red gravelly sandstone and mudstone that unconformably overlie Cretaceous and pre-Cretaceous bedrock (Dai et al., 2005). The age of this stratigraphic unit was suggested to be Oligocene, on the basis of the presence of *Anagalopsiskansuensis* and *Mimolagusrodens* fossils and observed magnetic chrons (Bohlin, 1951; Dai et al., 2005).

The overlying Baiyanghe Formation is dominated by purple-red mudstone with green-white gypsum layers throughout the Hexi Corridor basin; the presence of pollen fossils (including *Lycopodium* sp., *Podocarpus* sp., *Compositaceae*, *Polypodiaceae*, and *Betulaceae*) and magnetostratigraphy data (Wang et al., 2016a) constrain it to be late Oligocene to early Miocene.

The Shulehe Formation has been subdivided into three members, the Gongxingshan, Getanggou, and Niugetao. The Gongxingshan and the Getanggou Members are mostly characterized by alternating sandy conglomerate-sandstone-siltstone-mudstone cycles. The Niugetao Member consists mainly of sandstones and conglomerates (Fang et al., 2005). Above the Shulehe Formation, the Yumen and the Jiuquan conglomerates are dominated by >100-m-thick yellowish-gray conglomerates along the northern Qilian Shan in the southern basin margins. On the basis of the palynological assemblages, ostracod fossils, and magnetostratigraphy, the ages of the Shulehe Formation and Yumen and Jiuquan conglomerates are commonly suggested to be Miocene to early Pliocene, Pliocene, and Quaternary, respectively (Fang et al., 2005; Wang et al., 2016a).

SAMPLING AND MEASURING

In order to test the possible spatial variations of the history and degree of Cenozoic exhumation across the north Qilian Shan region, two different sampling strategies were designed. The first is to use the degree of annealing of fission tracks in local basement rocks to reveal the exhumation degree and the cooling history. The cooling history can then be

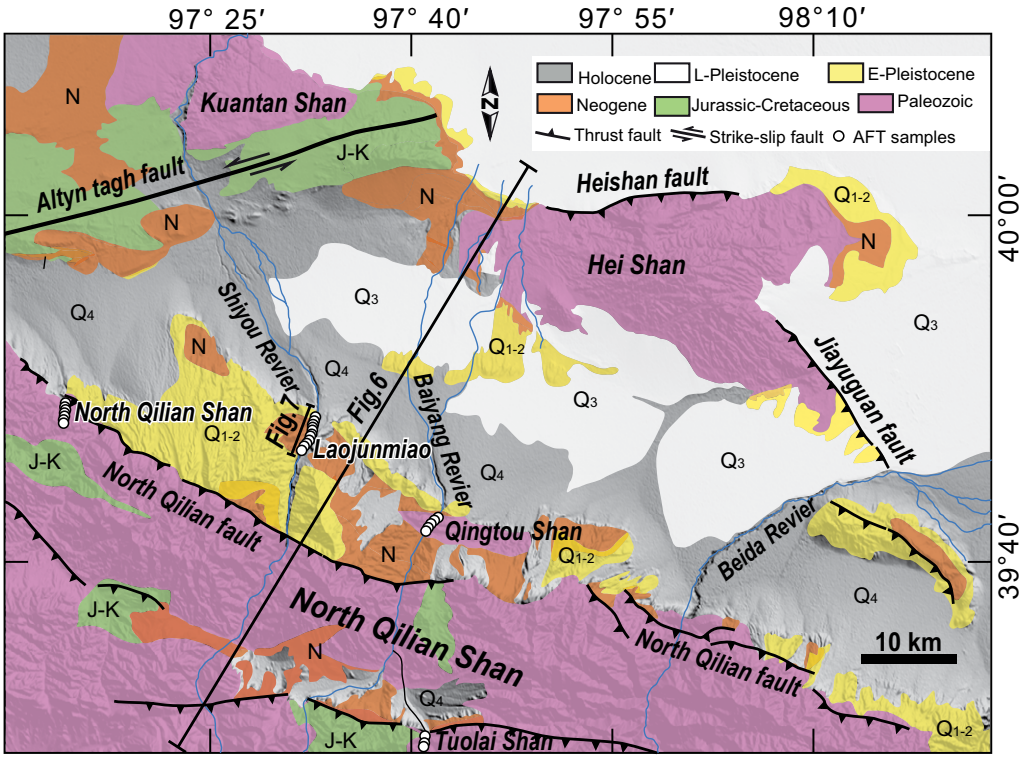

Figure 2. Geological map of northern Qilian Shan and Yumen Basin showing the main faults in the study region and the locations (white circles) of the apatite fission track (AFT) samples from the Tuolai Shan, northern Qilian Shan, Qingtou Shan, and the Laojunmiao anticline. The location of Figure 2 is shown in Figure 1. E—early; L—late.

employed to study the deformation history. The second sampling strategy we employed involved detrital sample collections from Cenozoic sediments in the Yumen Basin to trace their source age variations by detrital fission tracks. The detrital samples were collected along the Laojunmiao (LJM) section (Fig. 3) because the sediments in the section are well constrained by magnetostratigraphy (Fang et al., 2005). The LJM section crops out along the north limb of the anticline and is composed of ~2000 m of continuous Cenozoic strata (Fig. 3). These strata have been subdivided into five stratigraphic units: from the base to the top, the Gongxingshan, Getanggou, and Niugetao Members of the Shulehe Formation, and the Yumen and Jiuquan conglomerates. The depositional ages of these stratigraphic units are older than 13 Ma, older than 13 to 8.3 Ma, 8.3–4.9 Ma, 3.66–0.93 Ma, and 0.84–0.14 Ma, respectively (Fang et al., 2005). We collected 16 detrital samples from the LJM section (Fig. 3). We also mapped the LJM section in detail to place constraints on the timing of the formation of the growth strata in the LJM anticline using magnetostratigraphic age correlations.

The AFT samples were analyzed at the State Key Laboratory of Earthquake Dynamics, Institute of Geology, China Earthquake Administration. The AFT ages were obtained using the external detector method (Gleadow, 1981) and calculated by the zeta calibration method (Hurford and Green, 1983). Age-calibration standards are Durango apatite (31.4 ± 0.5 Ma) and Fish Canyon apatite (27.8 ± 0.2 Ma). CN5 glass was used to monitor neutron fluence during irradiation at the 492 reactor, China Institute of Atomic Energy. A CN5 apatite zeta calibration factor (Hurford and Green, 1983) of 352.5 ± 10 was used in age calculation. Spontaneous fission tracks in apatite were etched in 5.5% HNO_3 at 21 °C for 20 min (Donelick et al., 1999). Induced fission tracks in the low-U muscovite external detectors that covered apatite grain mounts and glass dosimeters during the irradiation were later etched in 40% HF at 20 °C for 40 min. Fission tracks and track length measurements were counted on a Zeiss microscope at 1000× magnification under dry objectives for apatite.

RESULTS

Detrital AFT Data from the LJM Section

We analyzed 16 middle Miocene–Quaternary sandstone samples by the AFT method. The results are presented in Table 1. Resulting ages were decomposed into statistically significant age populations (Table 1) using freely available binomial peak fitting (Brandon, 2002; see http://earth.geology.yale.edu/~markb/Software/FT_PROGRAMS/BinomFit). Partial resetting of the AFT ages can be ruled out, because sediment thicknesses of ~2 km are too low to produce sufficient burial heating. The depositional ages of samples were correlated to the magnetostratigraphic age dated by Fang et al. (2005). When we estimated the depositional ages, the bottom and top ages of each stratigraphic unit were used as primary markers, then the thickness relative to the top or base of the unit was used to interpolate the ages. The error of depositional ages for our samples is <1 m.y.

The lag time is defined as the difference between the component ages and the depositional ages for a detrital mineral. If we assume a constant value of the transport time (grains were transported by river systems from the source to deposition basin), the lag time can be used to interpret the exhumation rate. A short lag time may represent an increase in the exhumation rate, whereas an increase in the lag time may represent a decrease in the exhumation rate. Because the exhumation depth is less than that of the apatite fission-track closure isotherm (George et al., 2001; Guo et al., 2009) and because partial annealing may artificially reduce the lag time estimate, we cannot interpret lag times as exhumation rates in a straightforward manner. Even though affected by lower exhumation depth, the lag time still can trace the changes in source using the youngest and second-youngest component ages, rather than estimating the exhumation rate.

We plotted the youngest and second-youngest component ages of each sample related to its depositional age in Figure 4. At the bottom of the section, the sample 04-Y-16 has a youngest component age of ca. 68.6 Ma

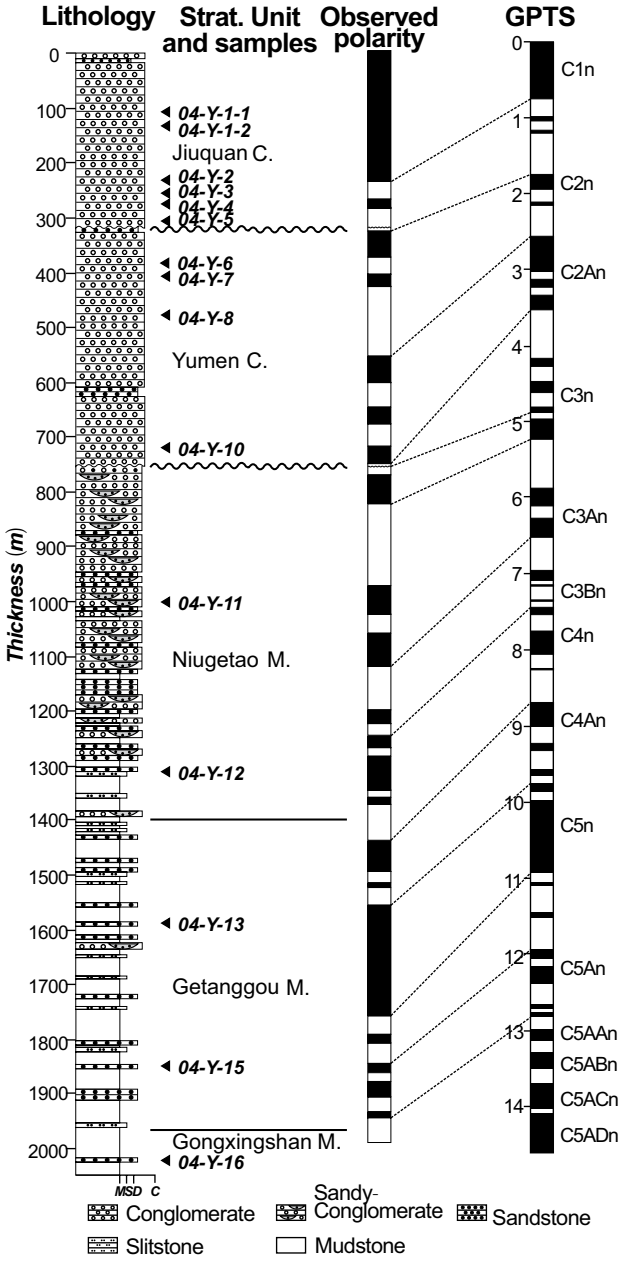

Figure 3. Stratigraphic (Strat.) column of the Laojunmiao (LJM) section with the detailed locations of the apatite fission track samples. The magnetostratigraphy of the LJM section and its correlations are from Fang et al. (2005). The Shulehe Formation is divided into the Gongxingshan, Getanggou, and Niugetao Members (M.). GPTS—geomagnetic polarity time scale.

and the second-youngest component age of 108.9 Ma (Table 1) with lag times of 54.6 Ma and 94.9 Ma, respectively. The youngest and second-youngest component ages of samples with a depositional age older than 10 Ma gradually decrease to 27.2 Ma and 60.7 Ma, and then the lag times shorten to 17.2 Ma and 50.7 Ma (sample 04-Y-13). A significant shift of the component age variation trend occurs near the middle of the section, between 8 and 10 Ma (between sample 04-Y-13 and 04-Y-12). For the samples with depositional ages between 8.0 and 2.0 Ma, the youngest and second-youngest component ages show upward increase trends from 29.4 Ma and 49.3 Ma to 65.5 Ma and 124.4 Ma (sample 04-Y-6). When the samples had depositional ages younger than 2.0 Ma, their youngest and second-youngest component ages decrease again from 65.5 Ma and 124.4 Ma to 40 Ma and 79.2 Ma, respectively (Fig. 4).

In general, the shorter lag time and the upsection decrease of the youngest and second-youngest component ages indicate progressive exhumation of a single source terrane. However, the overturn points of the lag time and of the youngest and second-youngest component age trends (from decreasing to increasing) suggest that the previous sediments were recycled. Thus, the depositional age corresponding to the overturn point could be the time when the sediment recycled.

In Figure 4, the decreasing values for the lag time and youngest as well as second-youngest component ages ca. 14–10 Ma represent progressive exhumation of the source ranges. The overturn points of the lag time and the youngest and second-youngest component age evolving trends ca. 10–8 Ma clearly show that sediment recycling happened at or before that time. The northern Qilian Shan is the nearest active mountain, which separates the Cenozoic sediments of the Hexi Corridor basin in the north from those of the Changma Basin in the south (Fig. 2). Therefore, we infer that the northern Qilian Shan thrust occurred ca. 10–8 Ma, and led to the deposits of the Changma Basin being recycled into the Hexi Corridor basin. This interpretation is consistent with the rapid uplift of the northern Qilian Shan ca. 9.5 Ma, as indicated by apatite helium data (Zheng et al., 2010).

Spatial Variation of Exhumation Degree

AFT ages from the base rocks are commonly used to date the onset of rapid cooling that is usually attributed to rock uplift and associated exhumation. The exhumation rate of a mountain therefore can be inferred based on the fission track (FT) ages. In this paper we use the AFT ages to estimate the exhumation degree because of the shallow exhumation of

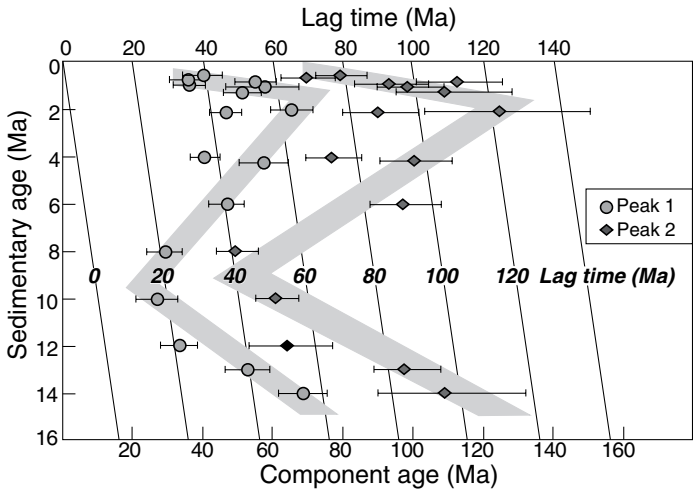

Figure 4. Apatite fission track (AFT) component ages versus depositional age plot. The circles are the youngest component ages (peak 1); the diamonds are the second-youngest component ages (peak 2). Prior to ca. 10 Ma, the youngest and second-youngest component ages decrease upward; however, after ca. 10–8 Ma, the youngest and the second-youngest component ages gradually increase with the depositional ages. The lag time shows a similar pattern. The overturn points of the youngest and the second-youngest component age trends and lag-time trend indicate that the previous sediments had recycled the new ones since ca. 10–8 Ma.

TABLE 1. DETRITAL APATITE FISSION TRACK DATA FROM THE LAOJUNMIAO SECTION

Sample	Depositional age (Ma)	N	Lag Time (Ma)	Age range (Ma)	P1			P2			P3		
					Peak age (Ma)	F (%)	W	Peak age (Ma)	F (%)	W	Peak age (Ma)	F (%)	W
04-Y-1-1	0.5	39	39.5	223.9–33.3	40.0 ± 5.5/6.4	4	23	79.2 ± 7.0/7.7	30	22	171.8 ± 20.8/23.6	5	22
04-Y-1-2	0.6	27	35.5	135.2–28.7	36.1 ± -5.0/5.8	8	32	69.6 ± 7.4/8.3	19	31			
04-Y-2	0.8	30	54.4	253.0–32.0	55.2 ± 5.8/6.4	15	27	112.6 ± 11.4/12.6	14	25	247.7 ± 53.7/68.2	1	28
04-Y-3	0.9	29	35.4	155.5–23.6	36.3 ± 4.3/4.9	14	33	93.0 ± 10.0/11.2	15	28			
04-Y-4	1.0	33	56.7	147.9–42.9	57.7 ± 9.5/11.3	7	28	98.4 ± 9.0/9.9	26	20			
04-Y-5	1.2	29	50.2	132.5–29.7	51.4 ± 5.1/5.6	20	27	108.9 ± 14.0/16.1	9	28			
04-Y-6	2.0	30	63.5	147.5–39.7	65.5 ± 5.9/6.4	27	24	124.4 ± 21.3/25.7	3	23			
04-Y-7	2.1	30	44.7	149.9–25.3	46.8 ± 4.3/4.7	22	22	89.8 ± 10.3/11.6	8	23			
04-Y-8	2.5	30	38.3	141.7–22.4	40.8 ± 4.2/4.7	12	24	76.7 ± 7.6/8.4	18	24			
04-Y-10	4.2	30	53.5	155.7–37.3	57.7 ± 6.7/7.6	11	27	100.1 ± 9.9/10.9	19	25			
04-Y-11	6.0	30	41.2	160.8–31.1	47.2 ± 4.7/5.2	13	22	97.1 ± 9.6/10.6	18	26			
04-Y-12	8.0	32	21.4	160.6–18.6	29.4 ± 4.6/5.5	9	30	49.3 ± 5.6/6.3	18	25	91.5 ± 18.1/22.5	5	34
04-Y-13	10.0	36	17.2	154.6–19.4	27.2 ± 5.3/6.5	5	35	60.7 ± 5.9/6.5	29	29	121.2 ± 33.8/46.5	3	35
04-Y-14	12.0	37	21.6	145.8–27.9	33.6 ± 4.8/5.6	5	29	63.9 ± 10.8/12.9	13	25	93.1 ± 12.6/14.6	19	27
04-Y-15	13.0	32	40.0	325.3–36.6	53.0 ± 6.1/6.9	12	27	97.6 ± 9.1/10.0	19	21	327.9 ± 78.3/102.0	1	31
04-Y-16	14.0	29	54.6	132.2–39.4	68.6 ± 6.7/7.4	23	26	108.9 ± 19.2/23.2	6	30			

Note: Binomial peak-fit ages (P1–P3) were determined with BINOMFIT (Brandon, 2002) and are given with 95% confidence interval (note that these intervals are asymmetric). Depositional age is based on the magnetostratigraphy (Fang et al., 2005). N—total of grains counted; F—the fraction of the specific peak; W—relative standard deviation for a peak. Samples were dated with the external detector method with a zeta (CN5) of 353 ± 10 yr/cm^2.

the Qilian Shan region. The basis for the exhumation degree estimation is the FT annealing, which increases with burial temperature. Following an increase in burial temperature (*T*), AFT ages will decrease and the FT lengths will shorten, until all tracks are erased at sufficient depth (annealed, *T*max >~110–125 °C). When the crust deformed (thrusting or normal faulting), the partial or entire annealing profile was brought to surface, and the younger FT age, which was once located in a much deeper position, was uplifted to shallow, and therefore presents a higher exhumation degree.

For the basement rocks in the Qilian Shan region, we present the AFT ages from three parallel ranges: from south to north, the Tuolai Shan, the northern Qilian Shan, and the Qingtou Shan (Fig. 2). The AFT age data for these three ranges are presented in Table 2 and Figure 5. The 3 samples collected from the Tuolai Shan exhibit AFT ages of 33.1–15.9 Ma with elevation ranging from 3228 m to 3930 m (Table 2). In contrast, 5 Qingtou Shan samples yielded ages from 98.2 to 51.3 Ma with elevations from 2451 m to 2564 m (Table 2). In addition, the AFT ages of the northern Qilian Shan samples range from 80 to 16 Ma with elevation from 2470 to 2930 m (Guo et al., 2009). Our results show that youngest ages with highest elevations are in the Tuolai Shan, whereas the oldest ages with lowest elevations are in the Qingtou Shan (Fig. 5). The AFT ages of the samples from the northern Qilian Shan in the medium elevations are older than those of samples from the Tuolai Shan, but younger than those of samples from the Qingtou Shan.

Although it is difficult to estimate exhumation degrees of these mountain ranges quantitatively, the trend that the AFT ages increase with their

TABLE 2. FISSION TRACK DATA FROM TUOLAI SHAN AND QINGTOU SHAN

Sample	Long (°E)	Lat (°N)	Altitude (m)	Strata	Nc	$\rho_d(N_d)$ (×10^6 cm^{-2})	$\rho_s(N_s)$ (×10^5 cm^{-2})	$\rho_i(N_i)$ (×10^6 cm^{-2})	U-Con. (ppm)	P(x^2) (%)	r	Fission track age (Ma ± 1σ)	ML ± 1σ (μm) (Nj)	SD (μm)
Tuolai Shan														
04-Y-33	97.63	39.38	3930	Anz	40	1.142 (2853)	1.472 (390)	0.934 (2476)	10.1	0.2	0.783	33.1 ± 3.7	13.06 ± 0.15 (80)	1.36
04-Y-34-1	97.69	39.50	3228	Anz	40	1.138 (2845)	0.394 (110)	0.460 (1284)	5.0	0.0	0.322	17.6 ± 4.5	13.31 ± 0.24 (24)	1.19
04-Y-34-2	97.69	39.50	3228	Anz	37	1.135 (2837)	0.962 (303)	1.598 (5034)	17.3	0.0	0.482	15.9 ± 4.0	13.76 ± 0.19 (53)	1.14
Qingtou Shan														
04-Y-37	97.69	39.70	2564	J	40	1.126 (2812)	3.176 (1245)	0.872 (3417)	9.5	0.0	0.772	98.2 ± 12.0	13.24 ± 0.12 (80)	1.10
04-Y-39	97.68	39.69	2590	D	34	1.265 (3161)	3.066 (699)	1.189 (271)	11.6	0.0	0.741	71.1 ± 9.6	13.73 ± 0.15 (69)	1.26
04-Y-40	97.69	39.70	2491	P2	30	1.259 (3148)	3.868 (1114)	1.284 (3698)	12.5	0.0	0.660	75.2 ± 8.6	13.15 ± 0.16 (70)	1.38
04-Y-41	97.69	39.70	2478	P2	30	1.132 (2831)	2.514 (724)	1.045 (3010)	11.4	0.0	0.620	51.3 ± 6.1	13.13 ± 0.11 (70)	0.99
04-Y-44	97.70	39.71	2451	C2	33	1.122 (2805)	3.084 (916)	1.246 (3702)	13.7	0.0	0.840	58.0 ± 7.1	13.49 ± 0.13 (63)	1.03

Note: Nc—number of dated apatite crystals per sample; N_d—number of induced fission tracks of dosimeter glass CN5; ρ_s—spontaneous track density; N_s—number of fission tracks counted; ρ_i—induced track density in external detector (muscovite); N_i—number of induced tracks counted; N_j—number of confined fission track lengths measured; U-Con.—uranium concentration; P(x^2)—chi-squared probability that all single-crystal ages represent a single population of ages where degrees of freedom = Nc-1; r—correlation coefficient between N_s and N_i; ML—mean confined fission track length with 1σ error; SD—standard deviation; Anz—Precambrian; D—Devonian; C2—Late Carboniferous; P2—Middle Permian; J—Jurassic.

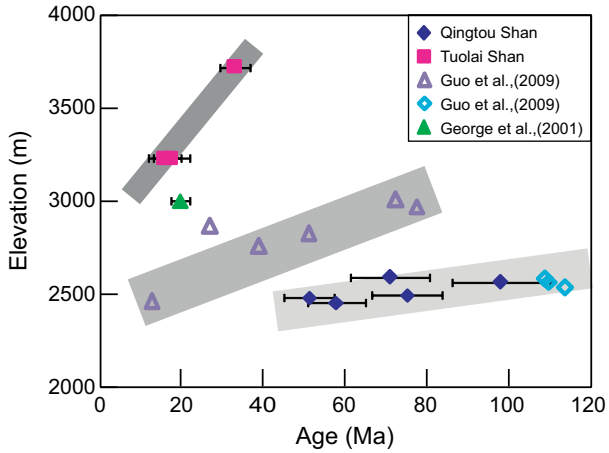

Figure 5. Spatial trends of apatite fission track ages, showing a gradually shallower exhumation of the ranges from south to north. The locations for the apatite fission track samples are shown in Figure 2. The squares are samples from Tuolai Shan; the triangles are samples from the northern Qilian Shan (filled—dated by George et al., 2001; unfilled—dated by Guo et al., 2009). The diamonds are samples from Qingtou Shan (filled—presented in this paper; unfilled—based on Guo et al., 2009).

elevations along any single section suggests that the reset zone has not yet reached the surface. However, among the different ranges, the older AFT ages with lower slopes in their age-elevation trends suggest a lower exhumation degree (Fig. 5). Thus, we can infer that degree of exhumation gradually decreases from the Tuolai Shan, to the northern Qilian Shan, and then the Qingtou Shan, based on sample AFT ages and their elevations (Fig. 5).

This inference is also consistent with the strata exposed in the study region (Figs. 2 and 6). The Tuolai Shan is largely composed of the Paleozoic and older metamorphic rocks with sparse Jurassic–Cretaceous fluvial-lacustrine sedimentary rocks. Northward, the northern Qilian Shan consists of Paleozoic metamorphic rocks, and some unconformably overlying Jurassic–Cretaceous fluvial-lacustrine sedimentary rocks. In particular, the Changma Basin, located between the Tuolai Shan and the northern Qilian Shan, contains Jurassic, Cretaceous, and Cenozoic sandstones and

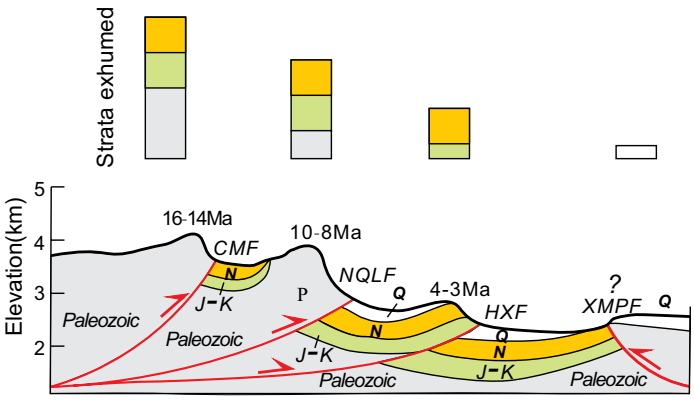

Figure 6. A simplified geologic cross section illustrating gradual northward shallowing exhumation in the study region suggested by the presence of the Mesozoic and Cenozoic strata. See Figure 2 for location of the cross section. CMF—Changma fault, NQLF—northern Qilian fault, HXF—Hexi fault, XMPF—Xinminpu fault.

mudstones. Farther north, the Hexi Corridor basin, which is in the north of the northern Qilian Shan, is mainly covered by Jurassic to Quaternary terrestrial rocks or sediments with only sparse outcrops of Paleozoic rocks. This kind of Jurassic–Cretaceous strata distribution pattern suggests that the Toulai Shan and the northern Qilian Shan probably had once been covered by the Jurassic–Cretaceous strata. The few remnant outcrops of Jurassic–Cretaceous strata currently preserved in the Toulai Shan and a gradual increasing in Jurassic–Cretaceous strata to the north suggest northward lower exhumation degrees in the study region (Fig. 6).

Growth Strata of the LJM Section

The LJM anticline is an asymmetrical fold; it has a gentle southern limb, but a very steep northern limb (Fig. 7A). This structure is controlled by the ramp of a blind thrust (Miaobei thrust). The oldest sedimentary rocks exposed along the LJM section are orange-red mudstones of the Baiyanghe Formation (early Miocene), which crop out at the core of the anticline. Along the northern limb of the anticline, middle Miocene to Quaternary yellowish mudstone, sandstone, and conglomerate beds are well exposed. We mapped the LJM anticline in detail from its core to the northern limb. Near the core, the Baiyanghe Formation dips to north with angles of ~65° (Fig. 7A). Northward to the upper part of the Niugetao Formation, the bedding dip angles are still larger than ~60°. Then, the dips of beds sharply decrease from ~60° to ~47° in the lower part of the Yumen conglomerates, suggesting that a syntectonic unconformity emerged (Fig. 7B). Farther north, the dips change from ~47° to 20° in the middle and upper parts of the Yumen conglomerates within a distance of 400 m, and then the dips of beds gradually decrease to 15° in the Jiuquan conglomerate (Fig. 7A). These phenomena indicate that a syntectonic unconformity was followed by the development of growth strata when the Yumen conglomerate and the Jiuquan conglomerate were deposited. This interpretation is also supported by the appearance of a coarsening-upward sequence of molasse deposits of the Yumen and Jiuquan conglomerates that may represent the initial deformation of the LJM anticline. Considering that the unconformity and growth strata initially appeared near the base of the Yumen conglomerate (4.9–3.6 Ma), the magnetostratigraphy of the LJM section can estimate the onset of deformation of the LJM anticline as 4.9–3.6 Ma.

DISCUSSION AND CONCLUSION

Both the exposed strata and the FT data from basement rocks suggest gradually lower exhumation degrees from south to north in the Qilian Shan region. Three reasons may explain the northward lower exhumation. First, the fault activity is weaker northward, i.e., the most intensive active fault in the study region is the Changma fault, which has the highest vertical moving speed of ~1 mm/yr (Institute of Geology, China Seismological Bureau and Lanzhou Seismological Institute, 1993). To the north, the northern Qilian Shan fault is a relatively active fault, with a long-term vertical speed of 0.5 mm/yr (Institute of Geology, China Seismological Bureau and Lanzhou Seismological Institute, 1993). The northernmost Qingtou Shan–LJM blind fault is the weakest active fault within the northern Qilian Shan thrust fault systems. Second, climate differences facilitate erosion through changes in precipitation. The Qilian Shan is located in an arid-semiarid area, but the northern Qilian Shan area undergoes intense erosion because of orographically enhanced precipitation (Pan et al., 2010). Third, the thrust deformation propagated progressively northward, i.e., the Tuolai Shan began to uplift first, then the northern Qilian Shan and the Qingtou Shan; the LJM anticline deformed last. The detrital AFT data collected from the northern Qilian Shan suggest that thrusting there began ca. 10–8 Ma; this is supported by apatite helium data, which reveal

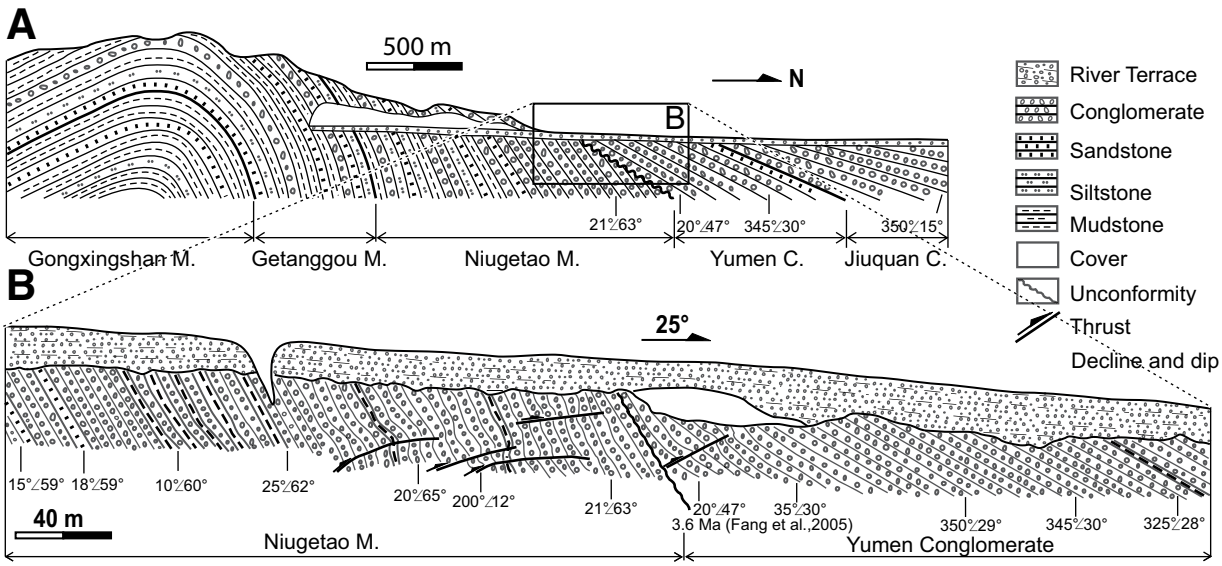

Figure 7. Geological mapping of the unconformity and growth strata along the Laojunmiao (LJM) section. The location of the LJM section is shown in Figure 2. (A) Profile of LJM anticline. (B) Detailed map of unconformity and growth strata in the upper part of the LJM section. The time of onset growth strata is estimated as ca. 4.9–3.6 Ma by magnetostratigraphy (Fang et al., 2005).

rapid exhumation of the northern Qilian Shan since ca. 9.5 Ma (Zheng et al., 2010). The syntectonic unconformity and growth strata in the LJM section indicate that the LJM anticline has deformed since 4.9–3.6 Ma. It is consistent with the cosmogenic data from Yumu Shan, which also is located in the northernmost part of the Qilian Shan region (Fig. 1). By dating the wind gap migrating, Palumbo et al. (2009) suggested that the onset of thrusting of the Yumu Shan fault probably took place ca. 3.6 Ma. Although the FT ages of the samples from the Tuolai Shan increase with elevation, those ages cannot provide a precise constraint on the onset time of Tuolai Shan deformation, because of small elevation differences between those samples. However, in Yuan et al. (2013) the previous results were summarized and it was concluded that the uplift of the Tuolai Shan may have initiated ca. 17–14 Ma, based on the slip rates of faults.

Exiting thermochronologic data cannot define the onset of uplift of the southern Qilian Shan; however, the formation of the Qaidam Basin in the south flank of the southern Qilian Shan in the Eocene and deposition of thick basal conglomerates (Yin et al., 2008; Zhuang et al., 2011), and initiation of the Hexi Corridor basin in the north flank of the southern Qilian Shan in the Oligocene and deposition of clasts from the south Qilian Shan (Bovet et al., 2009) seem to suggest that the growth of the southern Qilian Shan initiated in the Oligocene. In summary, the onset of deformation of the southern Qilian Shan, Tuolai Shan, and northern Qilian Shan and LJM anticline occurred in the Oligocene, 17–14 Ma, 10–8 Ma, and 4.9–3.6 Ma, respectively. We propose the progressively northward propagation model of the Qilian Shan growth, as shown in Figure 8.

Such progressive northward deformation processes in the Qilian Shan region broadly conform to the bathtub (Métivier et al., 1998; Meyer et al., 1998) or step-wise growth models of the Qilian Shan. Meyer et al. (1998) and Métivier et al. (1998) proposed a bathtub model for the growth of the Qilian Shan; they suggested that the southern Qilian Shan uplifted ca. 11 Ma, deformation progressively propagated northward, such that the deformation of the northern Qilian Shan occurred after 5 Ma, and

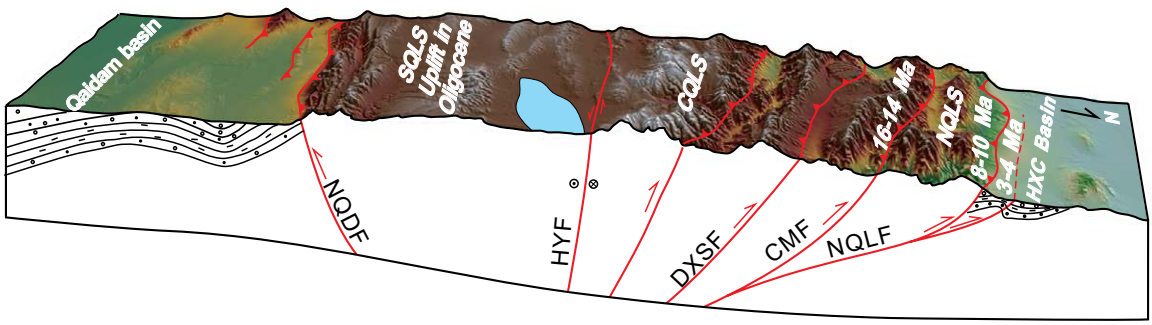

Figure 8. The progressive deformational model of the Qilian Shan in the Cenozoic. See Figure 1B for location of the swath. The southern part of the Qilian Shan uplifted probably since the Oligocene; deformation then propagated toward the north (Hexi Corridor basin) from the middle Miocene. HXC—Hexi Corridor basin, SQLS—southern Qilian Shan, CQLS—central Qilian Shan, NQLS—northern Qilian Shan, NQLF—northern Qilian fault, HYF—Haiyuan fault, CMF—Changma fault, NQDF—north Qaidam fault.

the deformation in the Hexi Corridor basin might have occurred in the Quaternary or later. Although this model generally describes the tectonic processes that happened in the Qilian Shan, the onset of single mountain range in the Qilian Shan region seems to be much earlier than the predictions of Meyer et al. (1998), Métivier et al. (1998), and Tapponnier et al. (2001).

The bathtub model of Meyer et al. (1998) and Métivier et al. (1998) linked the upward growth of the ranges in the Qilian Shan to Altyn Tagh fault activity in the late Miocene. However, the onset of the progressive northward growth of the Qilian Shan in the Oligocene is much earlier than the middle Miocene decrease of the left-lateral strike-slip rate on the Altyn Tagh fault (Yue et al., 2004), suggesting that the Oligocene growth of the southern Qilian Shan may reflect regional crustal shortening driven by the Qilian Shan thrust fault systems rather than accommodation of strike-slip movement on the Altyn Tagh fault. In addition, recent work on the formation of pull-apart basins located on the Altyn Tagh fault suggests that the full length of the fault was established before the Qilian Shan began shortening (Ritts et al., 2004). Geological observations also indicate that the Altyn Tagh fault may have extended beyond its current northeast tip into the Alxa region (Darby et al., 2005). These previous studies clearly show that the Altyn Tagh fault did not form as a structure to accommodate differential shortening between the Qilian Shan and Tarim Basin, but rather began serving in that capacity during the Miocene. Thus, we conclude that the progressive northward propagation of the Qilian Shan was induced by the Qilian Shan thrust fault systems, not by the Altyn Tagh fault.

ACKNOWLEDGMENTS

We are grateful for grants from the Strategic Priority Research Program of the Chinese Academy of Sciences (XDB03020200), and grants from the National Natural Science Foundation of China (41272215, 41030317, 41590861). Weitao acknowledges support from Professor Carmala Garzione and the Department of the Earth and Environmental Science, University of Rochester.

REFERENCES CITED

An, Z., Kutzbach, J.E., Prell, W.L., and Porter, S.C., 2001, Evolution of Asian monsoons and phased uplift of the Himalaya-Tibetan plateau since late Miocene times: Nature, v. 411, p. 62–66, doi:10.1038/35075035.

Bohlin, B., 1951, Some mammalian remains from Shih-ehr-ma-ch'eng, Hui-hui-p'u area, western Kansu, *in* Hedin, S., ed., Reports from the scientific expedition to the north-western provinces of China: Stockholm, Sino-Swedish Expedition Publication 35, p. 1–47.

Bovet, P.M., Ritts, B.D., Gehrels, G., Abbink, A.O., Darby, B., and Hourigan, J., 2009, Evidence of Miocene crustal shortening in the north Qilian Shan from Cenozoic stratigraphy of the western Hexi Corridor, Gansu Province, China: American Journal of Science, v. 309, p. 290–329, doi:10.2475/00.4009.02.

Brandon, M.T., 2002, Decomposition of mixed grain age distributions using BINOMFIT: On Track, v. 24, p. 13–18.

Burchfiel, B.C., Quidong, D., Molnar, P., Royden, L., Yipeng, W., Peizhen, Z., and Weiqi, Z., 1989, Intracrustal detachment within zones of continental deformation: Geology, v. 17, p. 748–752, doi:10.1130/0091-7613(1989)017<0448:IDWZOC>2.3.CO;2.

Champagnac, J.D., Yuan, D.Y., Ge, W.P., Molnar, P., and Zheng, W.J., 2010, Slip rate at the north-eastern front of the Qilian Shan, China: Terra Nova, v. 22, p. 180–187, doi:10.1111/j.1365-3121.2010.00932.x.

Clark, M.K., 2012, Continental collision slowing due to viscous mantle lithosphere rather than topography: Nature, v. 483, p. 74–77, doi:10.1038/nature10848.

Clark, M.K., Farley, K.A., Zheng, D., Wang, Z., and Duvall, A.R., 2010, Early Cenozoic faulting of the northern Tibetan Plateau margin from apatite (U–Th)/He ages: Earth and Planetary Science Letters, v. 296, p. 78–88, doi:10.1016/j.epsl.2010.04.051.

Dai, S., Fang, X., Song, C., Junping, G., Donglin, G., and Li, J., 2005, Early tectonic uplift of the northern Tibetan Plateau: Chinese Science Bulletin, v. 50, p. 1642–1652, doi:10.1360/03wd0255.

Darby, B.J., Ritts, B.D., Yue, Y., and Meng, Q., 2005, Did the Altyn Tagh fault extend beyond the Tibetan Plateau?: Earth and Planetary Science Letters, v. 240, p. 425–435, doi:10.1016/j.epsl.2005.09.011.

Donelick, R.A., Ketcham, R.A., and Carlson, W.D., 1999, Variability of apatite fission-track annealing kinetics: II. Crystallographic orientation effects: American Mineralogist, v. 84, p. 1224–1234, doi:10.2138/am-1999-0902.

Dupont-Nivet, G., Horton, B., Butler, R., Wang, J., Zhou, J., and Waanders, G., 2004, Paleogene clockwise tectonic rotation of the Xining-Lanzhou region, northeastern Tibetan Plateau: Journal of Geophysical Research, v. 109, B04401, doi:10.1029/2003JB002620.

Fang, X.-M., Zhao, Z.-J., Li, J.-J., Yan, M., Pan, B., Song, C., and Dai, S., 2005, Magnetostratigraphy of the late Cenozoic Laojunmiao anticline in the northern Qilian Mountains and its implications for the northern Tibetan Plateau uplift: Science in China Ser. D, Earth Sciences, v. 48, p. 1040–1051.

Fang, X., Zhang, W., Meng, Q., Gao, J., Wang, X., King, J., Song, C., Dai, S., and Miao, Y., 2007, High-resolution magnetostratigraphy of the Neogene Huaitoutala section in the eastern Qaidam Basin on the NE Tibetan Plateau, Qinghai Province, China and its implication on tectonic uplift of the NE Tibetan Plateau: Earth and Planetary Science Letters, v. 258, p. 293–306, doi:10.1016/j.epsl.2007.03.042.

Gansu Bureau of Geology and Mineral Resources, 1989, Regional geology of Gansu Province: Beijing, Geological Publishing House, 692 p.

George, A.D., Marshallsea, S.J., Wyrwoll, K.-H., Jie, C., and Yanchou, L., 2001, Miocene cooling in the northern Qilian Shan, northeastern margin of the Tibetan Plateau, revealed by apatite fission-track and vitrinite-reflectance analysis: Geology, v. 29, p. 939–942, doi:10.1130/0091-7613(2001)029<0939:MCITNQ>2.0.CO;2.

Gleadow, A., 1981, Fission-track dating methods: What are the real alternatives?: Nuclear Tracks, v. 5, p. 3–14, doi:10.1016/0191-278X(81)90021-4.

Guo, Z., Lu, J., and Zhang, Z., 2009, Cenozoic exhumation and thrusting in the northern Qilian Shan, northeastern margin of the Tibetan Plateau: Constraints from sedimentological and apatite fission-track: Acta Geologica Sinica, v. 83, p. 562–579, doi:10.1111/j.1755-6724.2009.00045.x.

Hetzel, R., Tao, M., Stokes, S., Niedermann, S., Ivy-Ochs, S., Gao, B., Strecker, M.R., and Kubik, P.W., 2004, Late Pleistocene/Holocene slip rate of the Zhangye thrust (Qilian Shan, China) and implications for the active growth of the northeastern Tibetan Plateau: Tectonics, v. 23, TC6006, doi:10.1029/2004TC001653.

Horton, B., Dupont-Nivet, G., Zhou, J., Waanders, G., Butler, R., and Wang, J., 2004, Mesozoic–Cenozoic evolution of the Xining-Minhe and Dangchang basins, northeastern Tibetan Plateau: Magnetostratigraphic and biostratigraphic results: Journal of Geophysical Research, v. 109, B04402, doi:10.1029/2003JB002913.

Hough, B.G., Garzione, C.N., Wang, Z., Lease, R.O., Burbank, D.W., and Yuan, D., 2011, Stable isotope evidence for topographic growth and basin segmentation: Implications for the evolution of the NE Tibetan Plateau: Geological Society of America Bulletin, v. 123, p. 168–185, doi:10.1130/B30090.1.

Hurford, A.J., and Green, P.F., 1983, The zeta age calibration of fission-track dating: Chemical Geology, v. 41, p. 285–317, doi:10.1016/S0009-2541(83)80026-6.

Institute of Geology, China Seismological Bureau and Lanzhou Seismological Institute, 1993, Qilian Mountain-Hexi Corridor active fault system: Beijing, Seismological Press, 340 p.

Jolivet, M., Brunel, M., Seward, D., Xu, Z., Yang, J., Roger, F., Tapponnier, P., Malavieille, J., Arnaud, N., and Wu, C., 2001, Mesozoic and Cenozoic tectonics of the northern edge of the Tibetan plateau: Fission-track constraints: Tectonophysics, v. 343, p. 111–134, doi:10.1016/S0040-1951(01)00196-2.

Lease, R.O., Burbank, D.W., Hough, B., Wang, Z., and Yuan, D., 2012, Pulsed Miocene range growth in northeastern Tibet: Insights from Xunhua Basin magnetostratigraphy and provenance: Geological Society of America Bulletin, v. 124, p. 657–677, doi:10.1130/B30524.1.

Métivier, F., Gaudemer, Y., Tapponnier, P., and Meyer, B., 1998, Northeastward growth of the Tibet plateau deduced from balanced reconstruction of two depositional areas: The Qaidam and Hexi Corridor basins, China: Tectonics, v. 17, p. 823–842, doi:10.1029/98TC02764.

Meyer, B., Tapponnier, P., Bourjot, L., Métivier, F., Gaudemer, Y., Peltzer, G., Shunmin, G., and Zhitai, C., 1998, Crustal thickening in Gansu-Qinghai, lithospheric mantle subduction, and oblique, strike-slip controlled growth of the Tibet plateau: Geophysical Journal International, v. 135, p. 1–47, doi:10.1046/j.1365-246X.1998.00567.x.

Molnar, P., and Tapponnier, P., 1975, Cenozoic tectonics of Asia: Effects of a continental collision: Science, v. 189, p. 419–426, doi:10.1126/science.189.4201.419.

Molnar, P., England, P., and Martinod, J., 1993, Mantle dynamics, uplift of the Tibetan Plateau, and the Indian monsoon: Reviews of Geophysics, v. 31, p. 357–396, doi:10.1029/93RG02030.

Molnar, P., Boos, W.R., and Battisti, D.S., 2010, Orographic controls on climate and paleoclimate of Asia: Thermal and mechanical roles for the Tibetan Plateau: Annual Review of Earth and Planetary Sciences, v. 38, p. 77–102, doi:10.1146/annurev-earth-040809-152456.

Palumbo, L., Hetzel, R., Tao, M., Li, X., and Guo, J., 2009, Deciphering the rate of mountain growth during topographic presteady state: An example from the NE margin of the Tibetan Plateau: Tectonics, v. 28, TC4017, doi:10.1029/2009TC002455.

Palumbo, L., Hetzel, R., Tao, M., and Li, X., 2010, Topographic and lithologic control on catchment-wide denudation rates derived from cosmogenic 10Be in two mountain ranges at the margin of NE Tibet: Geomorphology, v. 117, p. 130–142, doi:10.1016/j.geomorph.2009.11.019.

Pan, B.-T., Geng, H.-P., Hu, X.-F., Sun, R.-H., and Wang, C., 2010, The topographic controls on the decadal-scale erosion rates in Qilian Shan Mountains, NW China: Earth and Planetary Science Letters, v. 292, p. 148–157, doi:10.1016/j.epsl.2010.01.030.

Ritts, B.D., Yue, Y., and Graham, S.A., 2004, Oligocene–Miocene tectonics and sedimentation along the Altyn Tagh fault, northern Tibetan Plateau: Analysis of the Xorkol, Subei, and Aksay Basins: Journal of Geology, v. 112, p. 207–229, doi:10.1086/381658.

Royden, L.H., Burchfiel, B.C., King, R.W., Wang, E., Chen, Z., Shen, F., and Liu, Y., 1997, Surface deformation and lower crustal flow in eastern Tibet: Science, v. 276, p. 788–790, doi:10.1126/science.276.5313.788.

Royden, L.H., Clark, B., and van der Hilst, R.D., 2008, The geological evolution of the Tibetan Plateau: Science, v. 321, p. 1054–1058, doi:10.1126/science.1155371.

Tapponnier, P., Zhiqin, X., Roger, F., Meyer, B., Arnaud, N., Wittlinger, G., and Jingsui, Y., 2001, Oblique stepwise rise and growth of the Tibet Plateau: Science, v. 294, p. 1671–1677, doi:10.1126/science.105978.

Wang, W., Kirby, E., Peizhen, Z., Dewen, Z., Guangliang, Z., Huiping, Z., Wenjun, Z., and Chizhang, C., 2013, Tertiary basin evolution along the northeastern margin of the Tibetan Plateau: Evidence for basin formation during Oligocene transtension: Geological Society of America Bulletin, v. 125, p. 377–400, doi:10.1130/B30611.1.

Wang, W., Zhang, P., Pang, J., Garzione, C., Zhang, H., Liu, C., Zheng, D., Zheng, W., and Yu, J., 2016a, The Cenozoic growth of the Qilian Shan in the northeastern Tibetan Plateau:

A sedimentary archive from the Jiuxi Basin: Journal of Geophysical Research, v. 121, p. 2235–2257, doi:10.1002/2015JB012689.

Wang, W., Zhang, P., Yu, J., Wang, Y., Zheng, D., Zheng, W., Zhang, H., and Pang, J., 2016b, Constraints on mountain building in the northeastern Tibet: Detrital zircon records from synorogenic deposits in the Yumen Basin: Scientific Reports, v. 6, 27604, doi:10.1038/srep27604.

Wang, W., Zhang, P., Zheng, W., Zheng, D., Liu, C., Xu, H., Zhang, H., Yu, J., and Pang, J., 2016c, Uplift-driven sediment redness decrease at ~16.5 Ma in the Yumen Basin along the northeastern Tibetan Plateau: Scientific Reports, v. 6, 29105, doi:10.1038/srep29568.

Xiao, W., Windley, B.F., Yong, Y., Yan, Z., Yuan, C., Liu, C., and Li, J., 2009, Early Paleozoic to Devonian multiple-accretionary model for the Qilian Shan, NW China: Journal of Asian Earth Sciences, v. 35, p. 323–333, doi:10.1016/j.jseaes.2008.10.001.

Yin, A., and Harrison, T.M., 2000, Geologic evolution of the Himalayan-Tibetan orogen: Annual Review of Earth and Planetary Sciences, v. 28, p. 211–280, doi:10.1146/annurev.earth.28.1.211.

Yin, A., Rumelhart, P., Butler, R., Cowgill, E., Harrison, T., Foster, D., Ingersoll, R., Qing, Z., Xian-Qiang, Z., and Xiao-Feng, W., 2002, Tectonic history of the Altyn Tagh fault system in northern Tibet inferred from Cenozoic sedimentation: Geological Society of America Bulletin, v. 114, p. 1257–1295, doi:10.1130/0016-7606(2002)114<1257:THOTAT>2.0.CO;2.

Yin, A., Dang, Y.-Q., Zhang, M., Chen, X.-H., and McRivette, M.W., 2008, Cenozoic tectonic evolution of the Qaidam basin and its surrounding regions (Part 3): Structural geology, sedimentation, and regional tectonic reconstruction: Geological Society of America Bulletin, v. 120, p. 847–876, doi:10.1130/B26232.1.

Yuan, D.-Y., Zhang, P.-Z., Liu, B.-C., Gan, W., Mao, F., Wang, Z., Zheng, W., and Guo, H., 2004, Geometrical imagery and tectonic transformation of late Quaternary active tectonics in northeastern margin of Qinghai-Xizang Plateau: Acta Geologica Sinica, v. 78, p. 278–287 [in Chinese with English abstract].

Yuan, D.Y., Ge, W.P., Chen, Z.W., Li, C.Y., Wang, Z.C., Zhang, H.P., Zhang, P.Z., Zheng, D.W., Zheng, W.J., and Craddock, W.H., 2013, The growth of northeastern Tibet and its relevance to large-scale continental geodynamics: A review of recent studies: Tectonics, v. 32, p. 1358–1370, doi:10.1002/tect.20081.

Yue, Y., Ritts, B.D., and Graham, S.A., 2001, Initiation and long-term slip history of the Altyn Tagh fault: International Geology Review, v. 43, p. 1087–1093, doi:10.1080/00206810109465062.

Yue, Y., Ritts, B.D., Graham, S.A., Wooden, J.L., Gehrels, G.E., and Zhang, Z., 2004, Slowing extrusion tectonics: Lowered estimate of post–early Miocene slip rate for the Altyn Tagh fault: Earth and Planetary Science Letters, v. 217, p. 111–122, doi:10.1016/S0012-821X(03)00544-2.

Zhang, P., Molnar, P., and Downs, W.R., 2001, Increased sedimentation rates and grain sizes 2–4 Myr ago due to the influence of climate change on erosion rates: Nature, v. 410, p. 891–897, doi:10.1038/35073504.

Zhang, P.-Z., Shen, Z., Wang, M., Gan, W., Bürgmann, R., Molnar, P., Wang, Q., Niu, Z., Sun, J., and Wu, J., 2004, Continuous deformation of the Tibetan Plateau from global positioning system data: Geology, v. 32, p. 809–812, doi:10.1130/G20554.1.

Zheng, D., Zhang, P.-Z., Wan, J., Yuan, D., Li, C., Yin, G., Zhang, G., Wang, Z., Min, W., and Chen, J., 2006, Rapid exhumation at ~ 8 Ma on the Liupan Shan thrust fault from apatite fission-track thermochronology: Implications for growth of the northeastern Tibetan Plateau margin: Earth and Planetary Science Letters, v. 248, p. 198–208, doi:10.1016/j.epsl.2006.05.023.

Zheng, D., Clark, M.K., Zhang, P., Zheng, W., and Farley, K.A., 2010, Erosion, fault initiation and topographic growth of the North Qilian Shan (northern Tibetan Plateau): Geosphere, v. 6, p. 937–941, doi:10.1130/GES00523.1.

Zheng, W.-J., Zhang, P.-Z., He, W.-G., Yuan, D.-Y., Shao, Y.-X., Zheng, D.-W., Ge, W.-P., and Min, W., 2013a, Transformation of displacement between strike-slip and crustal shortening in the northern margin of the Tibetan Plateau: Evidence from decadal GPS measurements and late Quaternary slip rates on faults: Tectonophysics, v. 584, p. 267–280, doi:10.1016/j.tecto.2012.01.006.

Zheng, W.J., Zhang, P.Z., Ge, W.P., Molnar, P., Zhang, H.P., Yuan, D.Y., and Liu, J.H., 2013b, Late Quaternary slip rate of the South Heli Shan fault (northern Hexi Corridor, NW China) and its implications for northeastward growth of the Tibetan Plateau: Tectonics, v. 32, p. 271–293, doi:10.1002/tect.20022.

Zhuang, G., Hourigan, J.K., Ritts, B.D., and Kent-Corson, M.L., 2011, Cenozoic multiple-phase tectonic evolution of the northern Tibetan Plateau: Constraints from sedimentary records from Qaidam basin, Hexi Corridor, and Subei basin, northwest China: American Journal of Science, v. 311, p. 116–152, doi:10.2475/02.2011.02.

MANUSCRIPT RECEIVED 6 JULY 2016
REVISED MANUSCRIPT RECEIVED 21 DECEMBER 2016
MANUSCRIPT ACCEPTED 3 FEBRUARY 2017

Printed in the USA